Experimental diagnostic of sequence-variant dynamic perturbations revealed by broadband dielectric spectroscopy

Laëtitia Bourgeat, Lorenza Pacini, Anatoli Serghei, Claire Lesieur

Short article

Structure

Experimental diagnostic of sequence-variant dynamic perturbations revealed by broadband dielectric spectroscopy

Graphical abstract

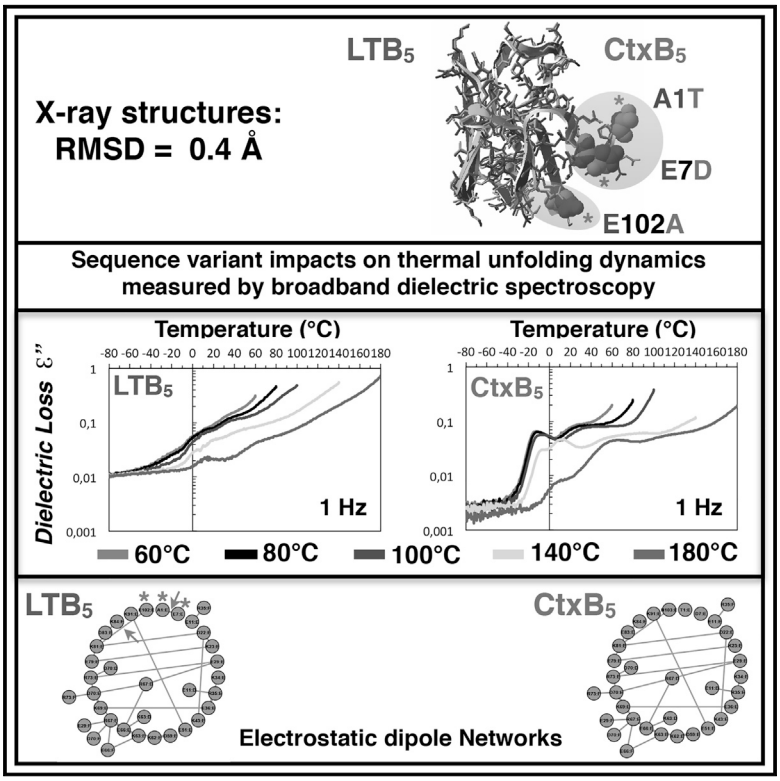

Authors

Laëtitia Bourgeat, Lorenza Pacini, Anatoli Serghei, Claire Lesieur

Correspondence

claire.lesieur@ens-lyon.fr

In brief

Genetic diversity designs proteins with sequence variants underlying robustness, adaptability and failure. Some variants maintain structural integrity but lead to disease, greater pathogen virulence, or drug resistance. Bourgeat et al. show, using two related toxin B-subunit pentamers, broadband dielectric spectroscopy and electrostatic networks that such variants have distinct thermal unfolding dynamics.

Highlights

- Broadband dielectric spectroscopy (BDS) monitors sequence-variant specific dynamics
- Electrostatic networks model dipoles involved in protein dielectric signals
- Nanoscale thermal unfolding of LTB- and CtxB-subunit pentamers monitored by BDS
- Sequence variants divert the two toxin B-subunits onto distinct unfolding routes

Bourgeat et al., 2021, Structure *29*, 1–11
October 7, 2021
https://doi.org/10.1016/j.str.2021.05.005

CellPress

Please cite this article in press as: Bourgeat et al., Experimental diagnostic of sequence-variant dynamic perturbations revealed by broadband dielectric spectroscopy, Structure (2021), https://doi.org/10.1016/j.str.2021.05.005

Structure

CellPress

Short article

Experimental diagnostic of sequence-variant dynamic perturbations revealed by broadband dielectric spectroscopy

Laëtitia Bourgeat,[1,3] Lorenza Pacini,[1,2] Anatoli Serghei,[3] and Claire Lesieur[1,2,4,*]
[1]Univ Lyon, CNRS, INSA Lyon, Université Claude Bernard Lyon 1, Ecole Centrale de Lyon, Ampère, UMR5005, 69622 Villeurbanne, France
[2]Institut Rhônalpin des systèmes complexes, IXXI-ENS-Lyon, 69007, Lyon, France
[3]Univ Lyon, CNRS, IMP, 69622, Villeurbanne, France
[4]Lead contact
*Correspondence: claire.lesieur@ens-lyon.fr
https://doi.org/10.1016/j.str.2021.05.005

SUMMARY

Genetic diversity leads to protein robustness, adaptability, and failure. Some sequence variants are structurally robust but functionally disturbed because mutations bring the protein onto unfolding/refolding routes resulting in misfolding diseases (e.g., Parkinson). We assume dynamic perturbations introduced by mutations foster the alternative unfolding routes and test this possibility by comparing the unfolding dynamics of the heat-labile enterotoxin B pentamers and the cholera toxin B pentamers, two pentamers structurally and functionally related and robust to 17 sequence variations. The B-subunit thermal unfolding dynamics are monitored by broadband dielectric spectroscopy in nanoconfined and weakly hydrated conditions. Distinct dielectric signals reveal the different B-subunits unfolding dynamics. Combined with network analyses, the experiments pinpoint the role of three mutations A1T, E7D, and E102A, in diverting LTB_5 to alternative unfolding routes that protect LTB_5 from dissociation. Altogether, the methodology diagnoses dynamics faults that may underlie functional disorder, drug resistance, or higher virulence of sequence variants.

INTRODUCTION

Genetic mutations have multiple effects on proteins. They design a diversity of sequence variants for a given protein, which yields protein robustness and adaptability. On one hand, the diversity supplies alternative functionally robust sequences and on the other, it enables functional innovation (Amitai et al., 2007; Laskowski and Thornton, 2008; McLaughlin et al., 2012; Ortlund et al., 2007; Wagner, 2012). This way, protein sustainability to time and conditions, relies on genetic mutations. Nevertheless, sequence variants can also have negative impacts and lead to functional failure and disease development, greater pathogen virulence, drug resistance, or cross-species transmission (Birkinshaw et al., 2019, p. 2; Ruberg and Berk, 2012; Vasile et al., 2014; Wu et al., 2020).

The default introduced by sequence variants can be of different natures: it may prevent protein synthesis, modify the 3D-structure or reproduce it but with different stabilities. Structural and stability faults are studied by both computational and experimental approaches (Degiacomi et al., 2013; Kamada et al., 2011; Lashuel et al., 1999; Mateu and Fersht, 1998).

There are also mutations that maintain structural integrity but prompt proteins to alternative unfolding/folding routes as observed in Alzheimer-like diseases (Ano Bom et al., 2012; Damas and Saraiva, 2000). We can assume the new routes to emerge from local modifications of the amino acid and atomic interactions at the sites of the mutations that do not disturb the overall structure, but alter the protein dynamics by propagating atomic motions in different directions within the protein structure. Because system dynamics and protein dynamics are susceptible to interaction (link) perturbations, this is a reasonable assumption (Battiston et al., 2012; Gheeraert et al., 2019; Unicomb et al., 2018).

Moreover, there is accumulating evidence, particularly for functional dynamics such as allostery, that fast local dynamics ($<\mu s$) propagate larger-scale motions in nonlinear and peer-to-peer fashions through multiple paths (Buchenberg et al., 2017; Ghosh and Vishveshwara, 2007; Leitner and Yamato, 2018; Liang et al., 2018; Taddese et al., 2020; Vuillon and Lesieur, 2015).

Here, we propose to test the hypothesis that local dynamic perturbations associated with mutations impact the large-scale dynamics of the protein and lead to alternative unfolding/folding routes. The key to this purpose is the use of broadband dielectric spectroscopy (BDS). First, BDS typical frequency ranges from 10^7 Hz down to 10^{-3} Hz, is suitable for investigations on the slow protein motions underlying unfolding/folding processes (microsecond to second timescale) (Henzler-Wildman and Kern, 2007; Munoz and Cerminara, 2016). Second, dielectric signals arise from dipole fluctuations, which depend on the local

Please cite this article in press as: Bourgeat et al., Experimental diagnostic of sequence-variant dynamic perturbations revealed by broadband dielectric spectroscopy, Structure (2021), https://doi.org/10.1016/j.str.2021.05.005

environment of the dipoles, features essential to distinguish local dynamics perturbations related to mutations (Kremer and Schönhals, 2002). Third, the dielectric signals also depend on the morphological organization of matter, features essential to distinguish the dynamics of different unfolding/folding intermediate hallmarks of alternative unfolding/folding routes (Kremer and Schönhals, 2002). Moreover, the BDS experiments are performed in nanoconfinement to reduce the conformational heterogeneity associated with macroscopic measurement, which could prevent the detection of local dynamic perturbations related to mutation. Finally, the experiments are done in weakly hydrated conditions to limit the contribution of the bulk solvent to the dielectric signal, which could also prevent the detection of local dynamics perturbations related to mutation. We have recently shown that BDS in nanoconfined and weakly hydrated conditions reveals the dynamics of short-life unfolding and assembly intermediates which populate during the thermal unfolding of the cholera toxin B pentamers ($CtxB_5$) (Bourgeat et al., 2019; Pacini et al., 2020).

Now, we report the dynamic changes that occur upon the thermal unfolding of the heat-labile B pentamers (LTB_5), a toxin closely related to $CtxB_5$, sharing 84% sequence identity, superimposable atomic structures, and similar functions (Hirst, 1995). Macroscopic investigations have shown that LTB_5 is more stable than $CtxB_5$. LTB_5 disassembles at 84°C at pH 7.0, whereas $CtxB_5$ disassembles at approximately 77°C at pHs 7.5 and 6.0 (Bhakuni et al., 1991; Goins and Freire, 1988; Ruddock et al., 1996b). LTB_5 pH-disassembly happens below pH 2.0 while $CtxB_5$ already disassembles at pH 3.9 (Ruddock et al., 1995). Non-native pentamers (SDS-sensitive) have been detected at pH 5.0 (De Wolf et al., 1987; Ruddock et al., 1996b). Assembly-competent and assembly-incompetent monomers have been detected as function of time in acid for both toxin B-subunits (Lesieur et al., 2002; Ruddock et al., 1996a). Refolding and reassembly studies show that the rate-limiting step in LTB_5 reassembly is a folding event involving the N-terminal (folding of the monomer or folding of the pentamer), whereas it is the interface formation involving histidine residues in $CtxB_5$ reassembly (Lesieur et al., 2002; Ruddock et al., 1996a; Zrimi et al., 2010). That is why the two toxin B-subunits that have superimposed atomic structures but different stability, unfolding and refolding mechanisms, are ideal candidates to test whether BDS which monitors slow dynamics (microsecond to second) can be used to investigate the impact of sequence variants on slow unfolding dynamics.

Our results show that the two B-subunits have different dielectric responses, and combined with network analyses, the role of two LTB_5-specific electrostatic dipoles, (A1, E7) and (K81, E102), introduced by the mutations A1T, E7D, and E102A, in protecting LTB_5 from chain dissociation is highlighted.

RESULTS

The slow molecular motions that take place upon the thermal unfolding of the cholera toxin B pentamer ($CtxB_5$) have been previously studied by BDS under nanoconfined and weakly hydrated conditions (Bourgeat et al., 2019; Pacini et al., 2020). We are now conducting the same investigation but for the heat-labile enterotoxin B pentamer (LTB_5) that shares 84% sequence identity, superimposable 3D structures (RMSD 0.41 Å), and similar function with $CtxB_5$ (Hirst, 1995). There are 17 amino acid substitutions in LTB_5 cf. $CtxB_5$: A1T S4N, E7D, S10A, Y18H, I20L, L25F, M31L, V38A, S44N, T75A, T80A, I82V, D83E, N94H, S95A, and E102A. These mutations do not impact the B-subunit structures and functions but make the LTB pentamers more stable and bring the two toxins to unfold and refold by different mechanisms.

The BDS experiments are performed as for $CtxB_5$, by solubilizing LTB_5 in PBS at pH 6.9 to have the electrostatic interactions that maintain a stable protein structure (Shoemaker et al., 2000; Vivian and Callis, 2001) (Methods) and be under ionized buffer conditions to have electrostatic dipoles as main contributors to the dielectric signal and nonionized dipoles negligible in comparison. The B-subunit samples are deposited on nanopores (40 nm diameter and 10 μm length) and the bulk water is evaporated at 50°C for 15 min, to avoid measuring bulk water dynamics (Methods).

Controls

LTB_5 is first incubated for 3 hours at 60°C and the dielectric loss ε'' of the sample measured as a function of temperature from 60°C to −80°C (cooling) and from −80°C back to 60°C (heating) (Figure 1A, C1). This first cycle (C1) is followed by a second incubation of the sample for 3 hours at 60°C, and measurement of the dielectric loss ε'' as a function of temperature from 60°C to −80°C (cooling) and from −80°C back to 60°C (heating) (Figure 1A, C2). The temperature dependency of the dielectric loss of the toxin is identical for the two cycles, indicating a steady sample containing mostly adsorbed water already after the first cycle and no more water evaporation during the second 3 hours of incubation at 60°C (Figure 1A). The superimposed signals also indicate that the unfolding has reached a steady state already after the first 3 hours at 60°C. The dielectric losses of the cooling (from 60°C to −80°C) and heating (−80°C–60°C) signals are also identical (Figure 1B). The absence of hysteresis indicates that after the 3 hours of incubation at 60°C, the conformational states of the sample are stable and no further unfolding/refolding can be detected dielectrically during the measurement. The cooling and heating signals are also superimposable after the treatments at 80°C, 100°C, and 140°C, so the same holds true (Figure 1B). Only the cooling measurement is performed after the thermal treatment at 180°C (Methods).

LTB_5 molecular dynamics

For proteins sensitive to heat, the mechanism of thermal unfolding leads to massive protein conformational changes from native functional states to unfolded and nonfunctional state. The thermal treatment induces a loss of amino acid and atomic interactions, releases geometrical constraints and triggers the propagation of thermal perturbations from local (amino acids) to larger spatial scales (e.g., quaternary, tertiary and secondary structures) that result in slow collective motions. The local environment of the dipoles will be impacted by the loss of the local atomic interactions and the morphology of the protein will be impacted by the larger-scale thermal perturbations, giving the possibility to study the toxin thermal unfolding by measuring the dynamic perturbations resulting from the thermal treatments using BDS.

Please cite this article in press as: Bourgeat et al., Experimental diagnostic of sequence-variant dynamic perturbations revealed by broadband dielectric spectroscopy, Structure (2021), https://doi.org/10.1016/j.str.2021.05.005

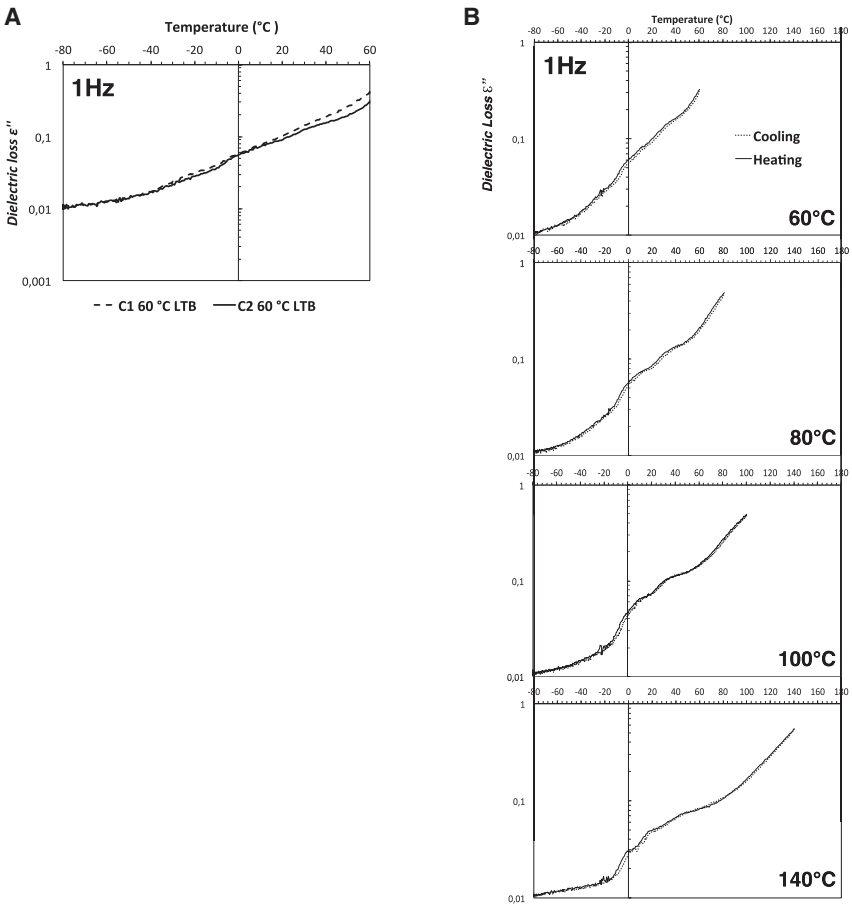

Figure 1. Toxin B-subunit sample stability

(A) The dielectric loss ε'' is plotted against temperature from 60°C to −80°C (cooling) after incubation of the toxin for 3 hours at 60°C (C1, Cycle 1) and after a second 3 hours of incubation at 60°C (C2, Cycle 2).

(B) The dielectric signal is measured from 60°C/80°C/100°C/140°C to −80°C (cooling) and from −80°C to 60°C/80°C/100°C/140°C (heating) after the second 3 hours incubation of the toxin at 60°C.

The temperature dependency of the dielectric loss of LTB-subunits is shown for the cooling measurements after the thermal treatments at temperatures from 60°C to 180°C (Figure 2). The linear increase in the dielectric loss ε'' with increasing temperature is due to the conductivity contribution of the sample while the nonlinear (i.e., peaks) increase is due to molecular relaxations (Kremer and Schönhals, 2002). The relaxation peaks correspond to the dynamics of the B-subunits detectable in the temperature and frequency windows of the measurements. After the thermal treatment at 60°C, the LTB_5 toxin dielectric loss ε'' is rather linear with temperature over the frequencies from 1 Hz to 1 MHz even though ill-defined peaks can be guessed at frequencies from 10 Hz to 1 kHz (Figure 2). The lack of signal shows that no electrostatic dipoles fluctuate within the frequency and temperature range of the experiment, meaning LTB_5 exhibits none of the slow collective fluctuations underlying folding/unfolding processes (Bourgeat et al., 2019; Munoz and Cerminara, 2016). This result also reveals that in absence of structural perturbations by the thermic treatment, the native toxin state presents no slow dynamics when not functioning, like in our experiments where the B-subunit function is not triggered. This is consistent with slow dynamics being a hallmark of protein folding/unfolding and protein functions while fast dynamics (nanosecond and below) involve local motions such as for example isolated side chain motions and bond vibrations (Henzler-Wildman and Kern, 2007; Munoz and Cerminara, 2016).

After the thermal treatment at 80°C, two relaxation processes are detected, P_{1L} over the frequencies from 1 Hz to 10 kHz and P_{2L} over the frequencies from 1 to 10 Hz (Figure 2), revealing collective dipole motions and the beginning of the LTB_5 thermal unfolding. The peaks are numbered from lower temperature positions (P_{1L}) to higher temperature positions (P_{2L}) and according to their appearance over the temperatures of the thermal treatments (Figure 2, 140°C P_{3L}). Moreover, the peaks are indexed L for LTB_5 samples.

After the thermal treatment at 100°C, there are few changes in the dielectric spectra indicating similar dynamics at 80°C and 100°C and thus no dielectrically detectable further unfolding despite the higher temperature of the thermal treatment.

After the thermal treatment at 140°C, P_{2L} is still detected but with less-defined peaks indicating the toxin further unfolding into conformations whose dynamics is no more detected within the frequency and temperature windows of our measurement as no new peak emerges from the disappearance of the P_{2L} peak (Figure 2). In contrast, the relaxation process P_{1L} exhibits a shoulder indicating also further unfolding but detected with the additional relaxation process P_{3L} (Figure 2). The P_{3L} peak emerges at lower temperature positions than the P_{1L} peak, indicating dipoles with faster fluctuations than the P_{1L} dipoles and therefore smaller collective motions (Figure 2, 140°C, arrow pointing to the left). Both relaxation peaks P_{1L} and P_{3L} are detected over the frequencies from 1 Hz to 10 kHz.

After the thermal treatment at 180°C, P_{1L} is still detected over the frequencies from 1 Hz to 1 MHz but P_{3L} is no longer detected (Figure 2). There is a new relaxation process, P_{4L} detected over the frequencies from 1 Hz to 10 kHz (Figure 2). The P_{1L} peak intensity decreases significantly, indicating that most of the toxin sample has unfolded into a new state with a different dynamics, possibly probed by the P_{4L} as its intensity is similar to the P_{1L} loss of intensity (Figures 2, 180°C, arrows). The temperature position of P_{4L} is shifted to higher temperature compared with P_{1L}, indicating dipoles with slower (more collective) motions in agreement with a more unfolded state where the local environment of the P_{1L} dipoles has changed. Alternatively, the P_{4L} relaxation might involve the fluctuation of electrostatic dipoles that were

Please cite this article in press as: Bourgeat et al., Experimental diagnostic of sequence-variant dynamic perturbations revealed by broadband dielectric spectroscopy, Structure (2021), https://doi.org/10.1016/j.str.2021.05.005

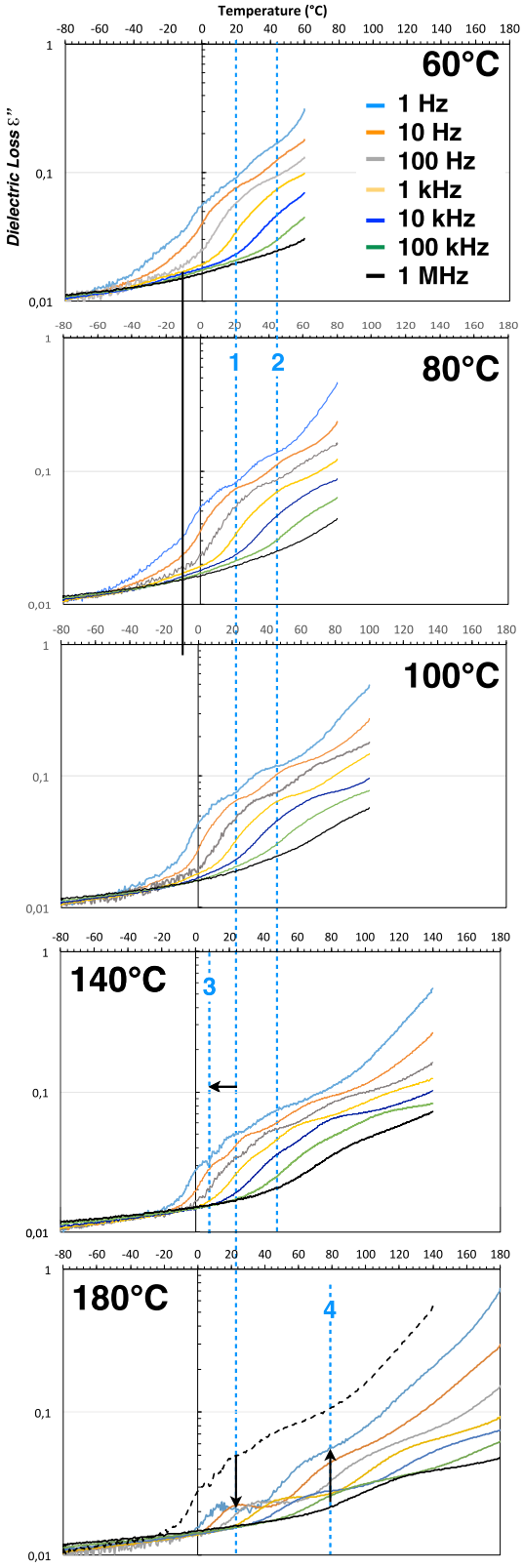

Figure 2. LTB_5 thermal dynamics changes

Temperature dependencies of the LTB_5 dielectric signals after successive thermal treatments from 60°C to 180°C and for frequencies from 1 Hz to 1 MHz. The vertical cyan dotted lines underline the 1 Hz temperature positions of the different relaxation peaks, identified by their respective numbers (e.g., P_{1L} = 1). In the 140°C plot, the arrow pointing to the left indicates the shift of temperature position between the relaxation peak P_{1L} and the relaxation peak P_{3L}. In the 180°C plot, the 1-Hz dielectric signal after the thermal treatment at 140°C is reported (black dotted line) to show the similarity of the drop of intensity of the Peak 1 between the 140°C and the 180°C thermal treatments (arrow pointing down) and the intensity of the Peak 4 (arrow pointing up), peak which appears following the thermal treatment at 180°C.

not disturbed at 140°C in which case the fluctuation of the P_{1L} dipoles might be outside the temperature and frequency windows of the experiment and fall out of detection at 180°C.

In summary, different relaxation processes respectively composed of different sets of dipoles are measured along the thermal treatments. This allows characterizing the unfolding of different areas of the toxin B-subunits via the fluctuations of their respective set of dipoles. The relaxation peaks P_{1L} are detected at higher temperature positions than the relaxation peaks P_{3L} and the relaxation peaks P_{2L} are detected at higher temperature positions than both the relaxation peaks P_{3L} and P_{1L}. This means P_{3L} involves dipoles with faster motions than the P_{1L} dipoles, which themselves involved dipoles with faster motions than the P_{2L} dipoles. In terms of spatial scales of motions, it implies P_{3L} detects smaller collective motions than P_{1L}, which detects smaller collective motions than P_{2L}. Moreover, the temperature positions of peaks shift to higher temperatures as the temperature of the thermal treatments increases consistently with more and more dipoles fluctuating (larger collective motions) as the protein unfolds more with the increase of the temperature of the thermal treatments.

LTB_5 molecular dynamics versus $CtxB_5$ molecular dynamics

As already mentioned, the dielectric data of the $CtxB_5$ samples for thermal treatments from 60°C to 180°C have been published and are partially reproduced here (Figure 3A, bottom panels) for the sake of comparison (Bourgeat et al., 2019; Pacini et al., 2020). The peaks are indexed C for the $CtxB_5$ samples.

In all the thermal treatments, the CtxB relaxation peaks are systematically better resolved than the LTB relaxation peaks indicating a higher dipole contribution for $CtxB_5$ and hence a higher population of unfolded molecules (Figure 3). The higher heat resistance of LTB_5 is also supported by the lack of relaxation processes at 60°C when $CtxB_5$ presents already two relaxation processes P_{1C} and P_{2C} (Figure 3A, bottom panel).

The comparison of the dielectric signals also shows that the two toxin pentamers follow different thermal unfolding paths (Figure 3B). The thermal unfolding of LTB_5 only starts at 80°C with two peaks detected P_{1L} and P_{2L}. On one hand, the P_{2L} and P_{2C} relaxation peaks detected at early stage of the thermal unfolding, have similar temperature dependencies (Figure 3A, vertical lines 2), indicating that the same set of dipoles hence the dynamics of the same toxin areas is probed (Figure 3B, dark gray area). Nevertheless, only the P_{2C} peaks are broad, in particular after the thermal treatment at 140°C, indicating dipoles with heterogeneous temperature dependencies and hence heterogeneous timescale fluctuations. Because chain dissociation produces protein assembly intermediates composed of monomers with interfaces and monomers with

Please cite this article in press as: Bourgeat et al., Experimental diagnostic of sequence-variant dynamic perturbations revealed by broadband dielectric spectroscopy, Structure (2021), https://doi.org/10.1016/j.str.2021.05.005

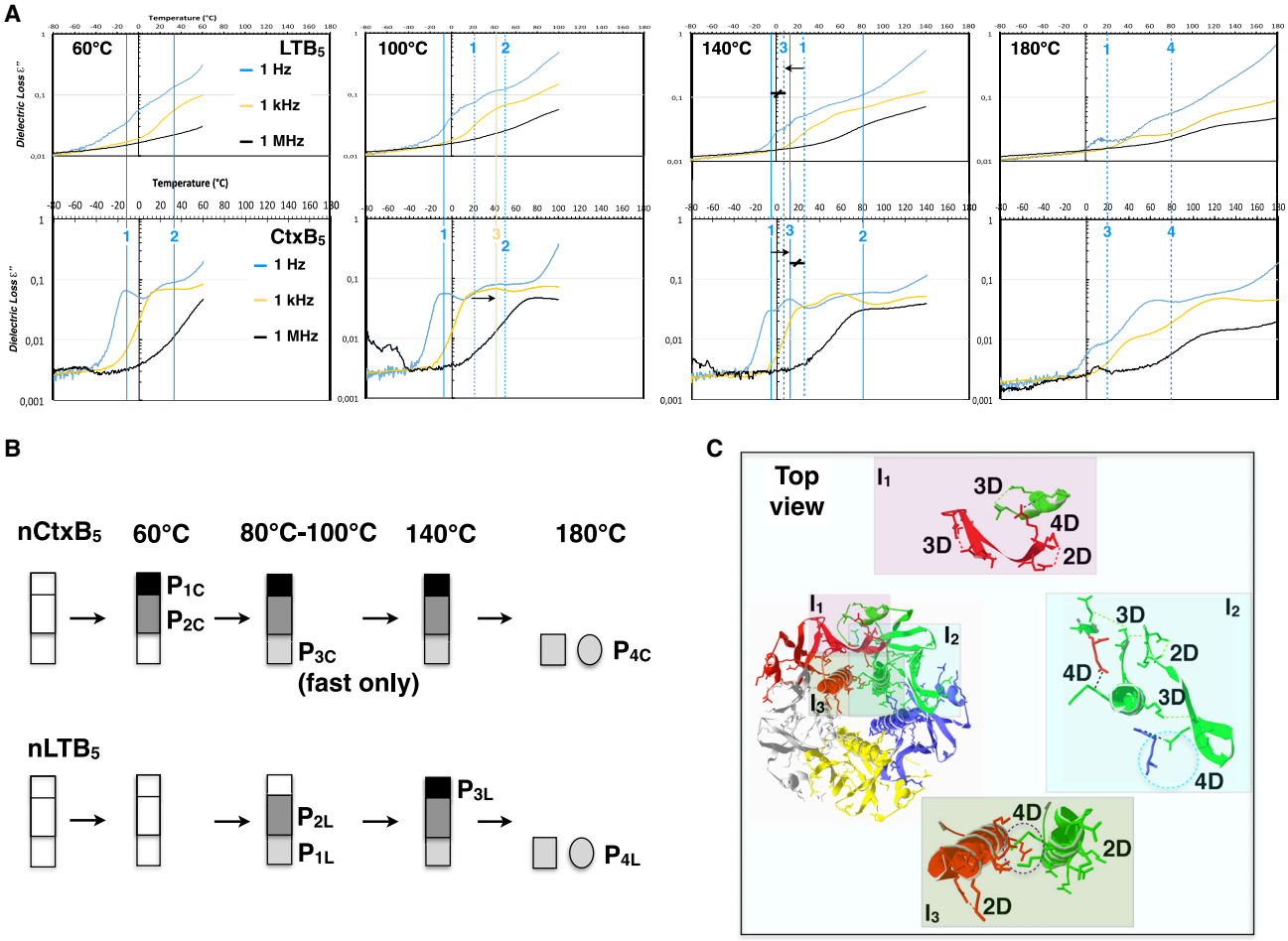

Figure 3. Thermal dynamics changes of LTB_5 and $CtxB_5$

(A) LTB_5 and $CtxB_5$ thermal dynamics changes measured by BDS. Temperature dependencies of the LTB_5 (top) and $CtxB_5$ (bottom) dielectric signals after the thermal treatments at different temperatures and for three different frequencies. The vertical lines underline the temperature positions of the different peaks for 1 Hz (cyan) and 1 kHz frequencies (orange), identified by their respective numbers. The dotted lines are for LTB_5 peaks while the continuous lines are for $CtxB_5$ peaks. The arrows illustrate the shift of the position in temperature of the new peaks emerging at higher temperatures of the thermal treatments (Peaks 3) compared to the peaks detected at lower temperatures (Peaks 1). The differences between the two toxin B-subunit peaks 1 and 3 which exhibit the presence of additional dipoles is illustrated with ▬.

(B) Schematics of the unfolding mechanisms based on the different relaxation peaks detected by BDS along the thermal treatments. The whole box represents the toxin and each smaller colored box schematizes the toxin area with the dipole fluctuations contributing to one relaxation peak. The white boxes depict the native state of the toxin pentamers, namely the structural state before the thermal unfolding starts, which is not detected in the experiments. The absence of boxes indicates a relaxation process no more detected, implying a structural state that cannot be identified because its dynamics fails outside the frequency and temperature windows of the experiments. The P_4 relaxation is illustrated as a conformational change resulting from the P_{3C} ($CtxB_5$) or P_{1L} (LTB_5) dipoles having different local environment after the thermal treatment at 180°C. Alternatively, the P_4 relaxation could arise from the fluctuations of new dipoles not destabilized at 140°C, in which case the toxin native state should be represented by four boxes instead of three.

(C) Charged amino acids in the X-ray structure of LTB_5 (PDB 1LTR). Each monomer of the pentamer is colored differently and the charged amino acids are depicted in stick atomic representation. Zooms in the three interface areas (I_1, I_2, and I_3) containing positive and negative charged amino acids close enough to make electrostatic dipoles (dotted lines) are shown. The electrostatic dipoles make: (1) contacts between different chains (4D contacts), (2) contacts within a chain between amino acids far away along the sequence (3D contacts), and (3) contacts within a chain between amino acids belonging to the same secondary structure element (2D contacts).

no interfaces, it naturally creates heterogeneous environment for intermolecular dipoles (two charged residues from different chains), a straightforward explanation for the heterogeneity underlying the large peak (Bourgeat et al., 2019). In comparison, a P_{2C} populated by monomeric states with heterogeneous dipole environments is harder to foresee, in particular given the broadness of the peaks, which would imply a large diversity of monomeric states. Moreover, the narrow P_{2L} peaks are consistent with pentamers being detected instead of assembly intermediates, in agreement with the higher heat resistance of LTB_5, which would prevent interface dissociation at the early stage of unfolding.

On the other hand, the P_{1C} appears at lower temperature positions than the P_{1L} (Figure 3A, vertical lines 1), indicating that the

Please cite this article in press as: Bourgeat et al., Experimental diagnostic of sequence-variant dynamic perturbations revealed by broadband dielectric spectroscopy, Structure (2021), https://doi.org/10.1016/j.str.2021.05.005

first unfolding stage detected for LTB_5 involves the fluctuations of larger collective domains (Figure 3B, light gray boxes) than the first unfolding stage detected for $CtxB_5$ (Figure 3B, black boxes).

A third relaxation process P_{3C} appears after the thermal treatment at 80°C (see in Pacini et al., 2020) and 100°C in $CtxB_5$ (Figure 3A, bottom) but only after the thermal treatment at 140°C for LTB_5 (Figure 3A, top). Moreover, P_{3C} is detected at higher temperature positions than P_{1C} (Figure 3A, bottom, arrow pointing to the right) while P_{3L} is detected at lower temperature positions than P_{1L} (Figure 3A, top, arrow pointing to the left). This indicates that in $CtxB_5$, the fluctuations of the small collective domains (P_{1C}) resulting from the thermal treatments at low temperatures (Figure 3B, black boxes) propagate and lead to the fluctuations of larger collective domains (Figure 3B, light gray boxes) at higher temperatures of the thermal treatments (P_{3C}). Either the reverse happens for the LTB_5 thermal unfolding, large collective motions at low temperatures precede small collective motions at high temperatures or the low resolution of the LTB_5 dielectric signal prevent the detection of the P_{3L} relaxation process at low temperature of the thermal treatment, because the signal overlaps with the conductivity signal and with the P_{1L} signal (Figure 3B).

The P_{1C} relaxation peak is detected over the thermal treatments from 60°C to 140°C while the P_{1L} relaxation peak is detected from 80°C to 180°C, indicating that the domains that unfold at low temperatures have different heat resistance in the two toxin B-subunits (Figure 3A). Likewise, the P_{3L} is only observed transiently at 140°C while P_{3C} is observed from 80°C to 180°C (Figure 3A). The P_{1C} and the P_{3L} peaks have similar heat resistance and temperature positions of small-scale motions and likewise the P_{1L} and P_{3C} have heat resistance up to 180°C and temperature positions of larger-scale motions. This strongly suggests that P_{1C} and P_{3L} relaxations result from the fluctuations of common dipoles, as P_{3C} and P_{1L} do.

After the thermal treatment at 180°C, the third relaxation processes are still detected with a fourth relaxation peak P_{4C} and P_{4L} for $CtxB_5$ and LTB_5, respectively (Figure 3A). Both relaxation peaks have the same temperature positions in both the toxin B-subunits, indicating that the fluctuations of the same B-subunit areas are detected and suggesting that the B-subunits end in similar unfolded states, at least in terms of dielectric features, despite having followed different unfolding routes (Figure 3B).

The next question is to determine which mutated positions are responsible for the different stabilities and unfolding paths and more precisely which could make one area unfold at low temperature in one toxin but at high temperature in the other.

Network analyses unraveling LTB_5 and $CtxB_5$ molecular dynamics differences

In our previous study, amino acid network and intermolecular electrostatic dipole network of $CtxB_5$ (Methods) built from the toxin X-ray structure (PDB 1EEI), were used to analyze the toxin dielectric signals in structural terms (Bourgeat et al., 2019; Pacini et al., 2020). The experiments being performed in weakly hydrated (no bulk solvent) and nanoconfined conditions, the peaks were not analyzed in terms of α (structural relaxation of the bulk solvent), β and δ relaxations (local water relaxations) as usually done for BDS (Khodadadi et al., 2008; Olsson et al., 2020; Schiro et al., 2009). Literature on protein dynamics reports that small collective motions such as secondary (2D) and tertiary (3D) structure elements cover microsecond to millisecond timescale while larger collective motions such as domains, interfaces, and chains cover millisecond to second timescale (Henzler-Wildman and Kern, 2007; Munoz and Cerminara, 2016; Taddese et al., 2020). Accordingly, we concluded that the peaks P_{1C} and P_{3C}, detected over the frequencies from 1 Hz to 1 MHz (i.e., second to microsecond timescale fluctuations), involved fast dipole fluctuations from small collective 2D- and 3D-structure motions to slow dipole fluctuations from large domain or 4D-structural motions (interfaces/chain) while the peak P_{2C} involved only slow dipole fluctuations from large domain or 4D-structure motions.

We then simply assumed that the different relaxation processes reflected the distinct dynamics of unfolding and assembly intermediates that populate during the thermal unfolding of $CtxB_5$; intermediates characterized by the fluctuations of different sets of dipoles. In addition, as a first approximation, only intermolecular electrostatic dipoles (i.e., positive amino acids on one chain close enough to negative amino acids on another chain) were considered the main contributors to the signal. This is reasonable as the contribution of nonionized dipoles is negligible in ionized conditions and as the frequency range and the broadness of P_{2C} support the contribution of at least intermolecular dipoles to the signal. $CtxB_5$ has three zones of interface I_1, I_2, and I_3 whose stability was ranked according to their respective number of atomic and amino acid interactions and whose peak temperature position was attributed according to their respective number of intermolecular electrostatic dipoles (higher number of dipoles, higher temperature position for the peak). In brief, P_{1C} was attributed to the dynamics of a pentamer (narrow peak) with I_1 thermally destabilized but I_2 and I_3 intact; P_{3C} was a pentamer with no more I_1, I_2 destabilized, and I_3 intact, and finally P_{2C} was assembly intermediates with no more I_1 and I_2 but I_3 destabilized hence the dissociation upon the loss of the last I_3 interface in some monomers.

Following the same logic, to attribute conformations to the different peaks detected for the LTB_5 sample, the amino acid network and the intermolecular electrostatic dipole network of LTB_5 were built from the toxin X-ray structure (PDB 1LTR). LTB_5 has the same I_1, I_2, and I_3 interface areas than $CtxB_5$, each composed of electrostatic dipoles involved in secondary (2D), tertiary (3D), and quaternary (4D) structures, consistently with the detection of interface thermal destabilization by BDS over the frequencies from 1 Hz to 1 MHz (i.e., second to microsecond timescale fluctuations) (Figure 3C). The two toxin pentamer interface areas I_1, I_2, and I_3 are subdivided into spatially disconnected interfacial domains I_{1a}, I_{1b}, I_{2a}, I_{2b}, I_{2c}, and I_3, which have the same stability ranking and intermolecular electrostatic dipole content, inconsistently with the two different B-subunit dielectric signals (Table 1).

This suggests intramolecular electrostatic dipoles contribute to the dielectric signals as well, and are responsible for the differences. The electrostatic dipole network (EN) containing both intermolecular and intramolecular electrostatic dipoles was then built for the two toxin pentamers to investigate such possibility (Figure 4A) (Methods). The comparison of the ENs shows that LTB_5 has two supplementary intramolecular electrostatic dipoles (A1,

Please cite this article in press as: Bourgeat et al., Experimental diagnostic of sequence-variant dynamic perturbations revealed by broadband dielectric spectroscopy, Structure (2021), https://doi.org/10.1016/j.str.2021.05.005

Table 1. LTB_5 and $CtxB_5$ (underlined if different) interface interactions and intermolecular electrostatic dipoles inferred from the AAN and the 4D-EN (Methods)

Thermal Strength	Interfaces	Chain E[a]	Chain F[a]	Interface Parameter[b]	Chain D[a]	Interface Parameter[b]	Electrostatic Dipoles
Weak interfaces	I_{1a}	1–3	92–93	5, 50 5, 46			–
	I_{2c}	101–103	73–79 73–77	5, 65 5, 22			–
Moderate interfaces	I_{1b}	1–12	28–39	18, 139 19, 137			E11-R35
	I_{2b}	28–39			57–73 58–68	19, 157 19, 136	E29-R67
Strong interfaces	I_{2a}	25–32			88, 96-103	24, 166 26, 198	–
	I_3 Central α- helix: 61 to 81	61–77 63–77			63–81	12, 120 12, 97	E66-K63 E66-R67 D70-R67 R73-D70
		67–81	66–77	13, 90 12, 117			R67-E66 R67-D70 D70-R73

[a]The numbers refer to the first and last residue of each domain that constitutes the interface.
[b]Interface parameters: number of amino acid pairs, number of atomic interactions.

E7) and (K81, E102) compared with $CtxB_5$, due to the mutations A1T, E7D, and E102A at positions 1, 7, and 102 (Figure 4A). The ionized amino group of the N-terminal of the residue 1 is involved in the (A1, E7) dipoles (Methods). The electrostatic dipoles (K81, E102) are backup of the electrostatic dipoles (K81, N103), present in both toxin pentamers whereas the dipoles (A1, E7) have no backup in $CtxB_5$. The (K81, N103) dipoles are also present in LTB_5 although not shown on the LTB_5 network (Methods).

The (A1, E7) and (K81, E102) dipoles can be expected to increase the stability of the LTB_5 N-terminal and of the 3D-contacts between the β_6 (96–103) and the large central α-helix (59–79), respectively (Figure 4B), as salt bridges stabilize protein conformations (Xia et al., 2018). Moreover, the N-terminal is involved in the I_{1a} and I_{1b} interfaces (Table 1), so both interfaces can be expected to be more stable and less susceptible to dissociation in LTB_5 (Figure 4B). The (K81, E102) locks the lower end of the β_6 (96–103) into position with the large central α-helix (59–79) and the (A1, P93) locks the upper end of the β_6 into position with the I_{1a} interface (Figure 4B). Thus, the 3D-mobility of β_6, linked to the fluctuations of the dipoles (A1, E7) and (K81, E102) can be expected to be reduced in LTB_5. Likewise, the (K81, D22) dipoles lock the upper end of the β_2 (25–31) into position with the large central α-helix (59–79) while the intermolecular dipoles (D11, R35) lock the lower end of the β_2 into position with the I_{1b} interface, making the 3D mobility of the β_2 dependent as well on the dynamics of the additional dipoles (A1, E7) and (K81, E102) (Figure 4B). Since β_6 and β_2 on the adjacent chain compose the main β-interface (I_{2a}), the two supplementary dipoles are likely to also make I_{2a} less susceptible to dissociation in LTB_5 (Figure 4B). Finally, β_6 is connected intramolecularly to the α-helix (59–79) and the N-terminal such that a lower β_6 3D-mobility will also protect the I_3 interface (Figure 4B).

The network and structural analysis pinpoints that the two additional dipoles can stabilize the N-terminal, the C-terminal and the interfaces of LTB_5, consistently with a higher resistance to dissociation for LTB_5 and the attribution of the narrow peak P_{2L} to non-native-pentamers with destabilized interfaces but not enough for dissociation, and the attribution of the broad peak P_{2C} to assembly intermediates in CtxB. The network model also shows that the difference in the two toxin B-subunit dielectric signals is due to differences in the intramolecular dipole contents. Thus, our model of the CtxB thermal unfolding based on the first approximation that intermolecular dipoles are main dielectric contributors and hence oligomeric states are detected needs to be revisited. The contribution of intramolecular dipoles to the signal means that monomers can also be detected. Nevertheless, as the decrease of the intensity of the peaks with the temperature of the thermal treatments is not associated with the increase of intensity of a final peak, fully denaturated monomers are not captured and only transient intermediates are.

The peaks P_{4C}/P_{4L} have the highest temperature positions at the highest temperatures of the thermal treatments and hence correspond to the dynamics of the most denaturated states detected (largest-scale dynamics, highest thermal perturbation). The peaks P_{4C}/P_{4L} are the most likely peaks to monitor the dynamics of the B-subunit monomers, consistently with their lower signal intensities due to the loss of intermolecular dipoles and the loss of some of the intramolecular dipoles among which the (A1, E7) and (K81, E102), inferred from the lack of differences in the two B-subunit temperature positions of the P_4 peaks, compared to the P_1 and P_3 peaks (Figure 3A, 140°C, ➽).

The peaks P_{1C}/P_{3L} have the lowest temperature positions, hence the fastest dynamics, and can be attributed to the least denaturated state of the B-subunits detected; they are the most likely peaks thatmonitor the dynamics of native-like pentamers. In agreement with the detection of the P_{1C} peaks after the thermal treatment at 60°C for CtxB, temperature at which

Please cite this article in press as: Bourgeat et al., Experimental diagnostic of sequence-variant dynamic perturbations revealed by broadband dielectric spectroscopy, Structure (2021), https://doi.org/10.1016/j.str.2021.05.005

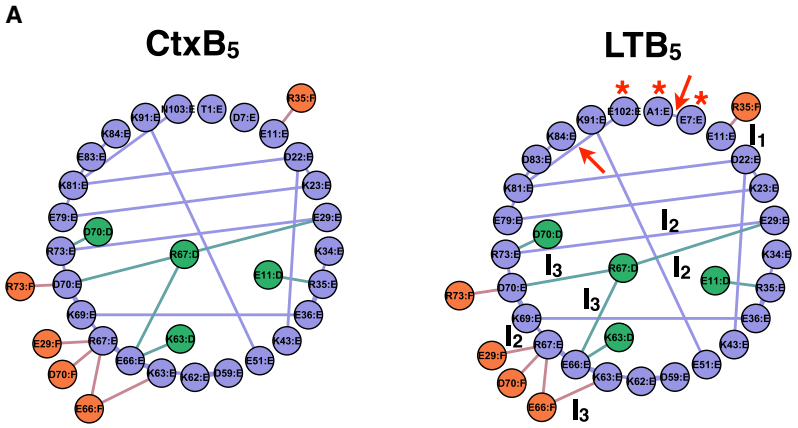

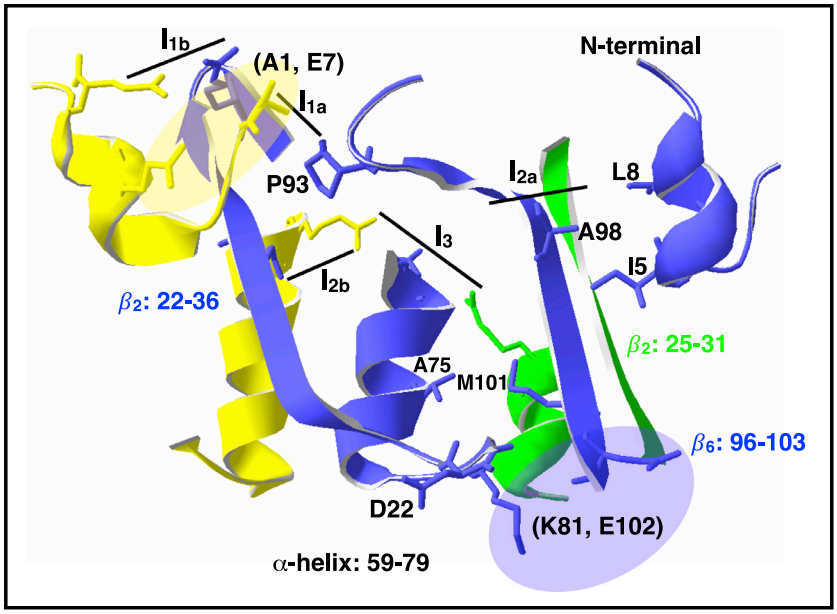

Figure 4. Structural analyses of the dynamic differences between LTB_5 and $CtxB_5$

(A) Electrostatic dipole networks of LTB_5 and $CtxB_5$. The red stars are for mutated position and the red arrows highlight electrostatic dipoles only present in LTB_5. I_1, I_2, and I_3 are the interface areas with intermolecular electrostatic dipoles.

(B) Positions of the additional dipoles (A1, E7) and (K81, E102) in the LTB_5 X-ray structure. The dipole (A1, E7) is located on the N-terminal domain, which is involved in the I_1 interfaces (I_{1a} and I_{1b}). The dipole (K81, E102) connects the β_6 from the main β-interface (I_{2a}, β_2: 25 to 31 and β_6: 96 to 103) to the tip of the central α-helix (residues 59 to 79) involved in the I_3 interface.

the B-subunit pentamers are not yet fully disassemble into monomers under macroscopic conditions (77°C for $CtxB_5$) (Bhakuni et al., 1991; Goins and Freire, 1988). P_{3L} is detected only after the thermal treatment at 140°C but that might be due to overlapping with the P_{1L} at lower temperatures, and we assume P_{3L} also monitors the dynamics of native-like LTB pentamers.

Under the new model and the new approximation, the P_{3C} peaks could be pentamers resulting from further interface destabilization at 140°C or monomers resulting from interface dissociation. However, the detection of the P_{1L} peaks after the thermal treatment at 80°C, tends to argue that the P_{1L} peaks monitor the dynamics of pentamers further unfolded than those monitored by the P_{3L} peaks since they have a higher temperature position, rather than the dynamics of monomers. Yet, the stronger interface associated with the two additional dipoles in LTB_5 could result in the promotion of unfolding within pentamers (narrow P_{2L}) instead of interface destabilization (broad P_{2C}), leading to a final cooperative interface dissociation into LTB monomers (P_{1L}) and no accumulation of assembly intermediates. The thermal perturbation of B-subunit pentamers would lead to accumulation of monomers at low temperature. LTB thermal unfolding would be driven by intramolecular perturbations while CtxB thermal unfolding would be driven by intermolecular perturbations, scenario which recalls the mechanisms of B-subunit reassembly where folding and association are rate-limiting in LTB and CtxB, respectively (Lesieur et al., 2002; Ruddock et al., 1996a).

A monomer is intuitively associated with a more unfolded state than native-like pentamers, non-native pentamers and assembly intermediates such that if the relaxation process P_{3C}/P_{1L} monitors monomer dynamics, it should exhibit larger-scale dynamics and have peaks at temperature positions higher than the relaxation processes P_{1C}/P_{3L} and P_{2C}/P_{2L}. The intermediate temperature position of the P_{3C}/P_{1L} peaks questions the attribution of the peak to monomers or it questions our "picture" of unfolded monomers. Of course, we know too little on such intermediates and their dynamics as well as on protein dielectric signals to settle this question at this stage. The key point is that the same peaks, not associated with the dynamics of fully denaturated monomers, are detected at temperatures below pentamer dissociation under macroscopic conditions and far above, showing the higher heat resistance of B-subunit pentamers and intermediate conformations under weakly hydrated conditions and nanoconfinement (Bhakuni et al., 1991; Goins and Freire, 1988; Ruddock et al., 1996b). Repeating the experiments using different nanoconfinements and different dehydration conditions will be one way to test the role of both parameters in the temperature-resistance of the toxin B-subunits. It must be noted that upon binding to the GM1-B-subunit receptor, $CtxB_5$ disassembles at 95°C showing already a resistance above 80°C (Goins and Freire, 1988). In addition, the introduction of an intermolecular disulfide bridge via the double mutant T1C-T92C (I_{1a} interface) makes $CtxB_5$ resistant to dissociation after

incubation with SDS and heating at 90°C and to pH 1.2 as the LTB pentamers, in agreement with our hypothesis that the dipole (A1, E7) by stabilizing the N-terminal stabilizes the I_{1a} interface and is responsible for the LTB_5 higher stability and lower interface dissociation (Miyata et al., 2012).

DISCUSSION

The LTB_5 and $CtxB_5$ dielectric signals are different demonstrating the capacity of the BDS to diagnose the impact of sequence variants on protein dynamics. The combination of the experimental results and the network analysis reveal the potential role of the two LTB_5-specific dipoles (A1, E7) and (K81, E102) and the mutations A1T, E7D, and E102A in deviating LTB_5 to unfolding paths that make LTB_5 more heat resistant and less prompt to thermal dissociation through assembly intermediates. This recalls what has been shown for the B-subunit *in vitro* reassembly under macroscopic conditions where the rate-limiting step for LTB_5 is a folding step involving the N-terminal but is interface formation involving the main β-interface (I_{2a}) for $CtxB_5$ (De Wolf et al., 1987; Lesieur et al., 2002; Ruddock et al., 1995, 1996a, 1996b; Zrimi et al., 2010). The concordance between the nanoscopic and the macroscopic investigations highlights the encoding of the dynamics (here the slow large-scale dynamics) in the sequence of proteins as does the distinct dielectric responses of the two toxin pentamers, and as shown by Anfinsen experiments in the early 1970s (Anfinsen, 1973). The large-scale dynamics being encoded in the protein sequences is in contradiction with other BDS investigation where the large-scale motions of proteins are described as slaved by the solvent (Frauenfelder et al., 2009; Olsson et al., 2020). In our experiments, the large-scale motions cannot be attributed to the bulk solvent because only protein-bound solvent remains when the measurements start. The dielectric features and the large-scale protein dynamics result from a mixture of pure protein dipoles and protein-solvent dipoles with dielectric contributions which depend on the local environment of the dipoles, similarly to what is described for Trp-fluorescence (Callis and Burgess, 1997).

Conclusion

We have shown that BDS under nanoconfined and weakly hydrated conditions can be used to investigate the impact of sequence variants on the dynamics involved in the B-subunits thermal unfolding. The dielectric features are analyzed according to the known molecular dynamics of the structural level of proteins and consistently with the model developed by L. A. Dissado and R. M. Hill where relaxation dynamics arise from the hierarchical organization of matter in structural clusters (Dissado and Hill, 1983). Heterogeneous conformations (broad peak) attributed to assembly intermediates and homogeneous conformations (narrow peak) attributed to non-native pentameric intermediates and/or monomers can be dielectrically characterized, offering an additional perspective to study the molecular dynamics underlying oligomerization and fiber formation. The possibility to measure slow protein dynamics experimentally makes BDS one of the few techniques that can be used to monitor the impact of sequence variants on functional dynamics, and diagnose the cause for disease development, increased virulence or drug resistance, a step toward personalized medicine.

STAR★METHODS

Detailed methods are provided in the online version of this paper and include the following:

- KEY RESOURCES TABLE
- RESOURCE AVAILABILITY
  - Lead contact
  - Material availability
  - Data and code availability
- EXPERIMENTAL MODEL AND SUBJECT DETAILS
- METHOD DETAILS
  - Materials
  - Protein sample preparation
  - Dielectric measurements
  - Control experiments
  - Electrostatic dipole network
- QUANTIFICATION AND STATISTICAL ANALYSIS

ACKNOWLEDGMENTS

We thanks the CNRS MITI for funding, Defi instrumentations aux limites ATTOGRAM.

AUTHOR CONTRIBUTIONS

L.B. and L.P. performed research and analyzed data, A.S. designed research, C.L. designed research, analyzed data, and wrote the manuscript.

DECLARATION OF INTERESTS

The authors declare no competing interests.

Received: December 14, 2020
Revised: March 23, 2021
Accepted: May 7, 2021
Published: May 28, 2021

REFERENCES

Amitai, G., Gupta, R.D., and Tawfik, D.S. (2007). Latent evolutionary potentials under the neutral mutational drift of an enzyme. HFSP J. *1*, 67–78.

Anfinsen, C.B. (1973). Principles that govern the folding of protein chains. Science *181*, 223–230.

Ano Bom, A.P., Rangel, L.P., Costa, D.C., de Oliveira, G.A., Sanches, D., Braga, C.A., Gava, L.M., Ramos, C.H., Cepeda, A.O., Stumbo, A.C., et al. (2012). Mutant p53 aggregates into prion-like amyloid oligomers and fibrils: implications for cancer. J. Biol. Chem. *287*, 28152–28162. https://doi.org/10.1074/jbc.M112.340638.

Battiston, S., Puliga, M., Kaushik, R., Tasca, P., and Caldarelli, G. (2012). DebtRank: too central to fail? Financial networks, the FED and systemic risk. Scientific Rep. *2*, 541. https://doi.org/10.1038/srep00541.

Bhakuni, V., Xie, D., and Freire, E. (1991). Thermodynamic identification of stable folding intermediates in the B-subunit of cholera toxin. Biochemistry *30*, 5055–5060.

Birkinshaw, R.W., Gong, J., Luo, C.S., Lio, D., White, C.A., Anderson, M.A., Blombery, P., Lessene, G., Majewski, I.J., and Thijssen, R. (2019). Structures of BCL-2 in complex with venetoclax reveal the molecular basis of resistance mutations. Nat. Commun. *10*, 1–10.

Bourgeat, L., Serghei, A., and Lesieur, C. (2019). Experimental protein molecular dynamics: broadband dielectric spectroscopy coupled with nanoconfinement. Sci. Rep. *9*, 17988. https://doi.org/10.1038/s41598-019-54562-8.

Buchenberg, S., Sittel, F., and Stock, G. (2017). Time-resolved observation of protein allosteric communication. Proc. Natl. Acad. Sci. U S A *114*, E6804–E6811.

Callis, P.R., and Burgess, B.K. (1997). Tryptophan fluorescence shifts in proteins from hybrid simulations: an electrostatic approach. J. Phys. Chem. B *101*, 9429–9432.

Damas, A.M., and Saraiva, M.J. (2000). TTR amyloidosis—structural features leading to protein aggregation and their implications on therapeutic strategies. J. Struct. Biol. *130*, 290–299.

De Wolf, M.J., Van Dessel, G.A., Lagrou, A.R., Hilderson, H.J., and Dierick, W.S. (1987). pH-induced transitions in cholera toxin conformation: a fluorescence study. Biochemistry *26*, 3799–3806.

Degiacomi, M.T., Iacovache, I., Pernot, L., Chami, M., Kudryashev, M., Stahlberg, H., Van Der Goot, F.G., and Dal Peraro, M. (2013). Molecular assembly of the aerolysin pore reveals a swirling membrane-insertion mechanism. Nat. Chem. Biol. *9*, 623–629.

Dissado, L.A., and Hill, R.M. (1983). A cluster approach to the structure of imperfect materials and their relaxation spectroscopy. Proc. R. Soc. Lond. A. Math. Phys. Sci. *390*, 131–180.

Dorantes-Gilardi, R., Bourgeat, L., Pacini, L., Vuillon, L., and Lesieur, C. (2018). In proteins, the structural responses of a position to mutation rely on the Goldilocks principle: not too many links, not too few. Phys. Chem. Chem. Phys. *20*, 25399–25410.

Frauenfelder, H., Chen, G., Berendzen, J., Fenimore, P.W., Jansson, H., McMahon, B.H., Stroe, I.R., Swenson, J., and Young, R.D. (2009). A unified model of protein dynamics. Proc. Natl. Acad. Sci. U S A *106*, 5129–5134.

Gheeraert, A., Pacini, L., Batista, V.S., Vuillon, L., Lesieur, C., and Rivalta, I. (2019). Exploring allosteric pathways of a V-type enzyme with dynamical perturbation networks. J. Phys. Chem. B *123*, 3452–3461.

Ghosh, A., and Vishveshwara, S. (2007). A study of communication pathways in methionyl-tRNA synthetase by molecular dynamics simulations and structure network analysis. Proc. Natl. Acad. Sci.U S A *104*, 15711–15716.

Goins, B., and Freire, E. (1988). Thermal stability and intersubunit interactions of cholera toxin in solution and in association with its cell-surface receptor ganglioside GM1. Biochemistry *27*, 2046–2052.

Henzler-Wildman, K., and Kern, D. (2007). Dynamic personalities of proteins. Nature *450*, 964–972.

Hirst, T.R. (1995). Biogenesis of Cholera Toxin and Related Oligomeric Enterotoxins (M. Dekker).

Kamada, R., Nomura, T., Anderson, C.W., and Sakaguchi, K. (2011). Cancer-associated p53 tetramerization domain mutants: quantitative analysis reveals a low threshold for tumor suppressor inactivation. J. Biol. Chem. *286*, 252–258. https://doi.org/10.1074/jbc.M110.174698.

Khodadadi, S., Pawlus, S., and Sokolov, A.P. (2008). Influence of hydration on protein dynamics: combining dielectric and neutron scattering spectroscopy data. J. Phys. Chem. B *112*, 14273–14280.

Kremer, F., and Schönhals, A. (2002). Broadband Dielectric Spectroscopy (Springer Science & Business Media).

Lashuel, H.A., Wurth, C., Woo, L., and Kelly, J.W. (1999). The most pathogenic transthyretin variant, L55P, forms amyloid fibrils under acidic conditions and protofilaments under physiological conditions. Biochemistry *38*, 13560–13573.

Laskowski, R.A., and Thornton, J.M. (2008). Understanding the molecular machinery of genetics through 3D structures. Nat. Rev. Genet. *9*, 141–151.

Leitner, D.M., and Yamato, T. (2018). Mapping Energy Transport Networks in Proteins (Wiley Online Library).

Lesieur, C., Cliff, M.J., Carter, R., James, R.F., Clarke, A.R., and Hirst, T.R. (2002). A kinetic model of intermediate formation during assembly of cholera toxin B-subunit pentamers. J. Biol. Chem. *277*, 16697–16704.

Liang, Z., Hu, J., Yan, W., Jiang, H., Hu, G., and Luo, C. (2018). Deciphering the role of dimer interface in intrinsic dynamics and allosteric pathways underlying the functional transformation of DNMT3A. Biochim. Biophys. Acta *1862*, 1667–1679.

Mateu, M.G., and Fersht, A.R. (1998). Nine hydrophobic side chains are key determinants of the thermodynamic stability and oligomerization status of tumour suppressor p53 tetramerization domain. EMBO J. *17*, 2748–2758.

McLaughlin, R.N., Jr., Poelwijk, F.J., Raman, A., Gosal, W.S., and Ranganathan, R. (2012). The spatial architecture of protein function and adaptation. Nature *491*, 138–142. https://doi.org/10.1038/nature11500.

Miyata, T., Oshiro, S., Harakuni, T., Taira, T., Matsuzaki, G., and Arakawa, T. (2012). Physicochemically stable cholera toxin B subunit pentamer created by peripheral molecular constraints imposed by de novo-introduced intersubunit disulfide crosslinks. Vaccine *30*, 4225–4232.

Munoz, V., and Cerminara, M. (2016). When fast is better: protein folding fundamentals and mechanisms from ultrafast approaches. Biochem. J. *473*, 2545–2559.

Olsson, C., Zangana, R., and Swenson, J. (2020). Stabilization of proteins embedded in sugars and water as studied by dielectric spectroscopy. Phys. Chem. Chem. Phys. *22*, 21197–21207.

Ortlund, E.A., Bridgham, J.T., Redinbo, M.R., and Thornton, J.W. (2007). Crystal structure of an ancient protein: evolution by conformational epistasis. Science *317*, 1544–1548.

Pacini, L., Bourgeat, L., Serghei, A., and Lesieur, C. (2020). Analysis of nanoconfined protein dielectric signals using charged amino acid network models. Aust. J. Chem. https://doi.org/10.1071/CH19502.

Ruberg, F.L., and Berk, J.L. (2012). Transthyretin (TTR) cardiac amyloidosis. Circulation *126*, 1286–1300.

Ruddock, L.W., Coen, J.J., Cheesman, C., Freedman, R.B., and Hirst, T.R. (1996a). Assembly of the B subunit pentamer of Escherichia coli heat-labile enterotoxin. Kinetics and molecular basis of rate-limiting steps in vitro. J. Biol. Chem. *271*, 19118–19123.

Ruddock, L.W., Ruston, S.P., Kelly, S.M., Price, N.C., Freedman, R.B., and Hirst, T.R. (1995). Kinetics of acid-mediated disassembly of the B subunit pentamer of Escherichia coli heat-labile enterotoxin. Molecular basis of pH stability. J. Biol. Chem. *270*, 29953–29958.

Ruddock, L.W., Webb, H.M., Ruston, S.P., Cheesman, C., Freedman, R.B., and Hirst, T.R. (1996b). A pH-dependent conformational change in the B-subunit pentamer of Escherichia coli heat-labile enterotoxin: structural basis and possible functional role for a conserved feature of the AB5 toxin family. Biochemistry *35*, 16069–16076.

Schiro, G., Cupane, A., Vitrano, E., and Bruni, F. (2009). Dielectric relaxations in confined hydrated myoglobin. J. Phys. Chem. B *113*, 9606–9613.

Shoemaker, B.A., Portman, J.J., and Wolynes, P.G. (2000). Speeding molecular recognition by using the folding funnel: the fly-casting mechanism. Proc. Natl. Acad. Sci. U S A *97*, 8868–8873.

Taddese, B., Garnier, A., Abdi, H., Henrion, D., and Chabbert, M. (2020). Deciphering collaborative sidechain motions in proteins during molecular dynamics simulations. Sci. Rep. *10*, 1–14.

Unicomb, S., Iñiguez, G., and Karsai, M. (2018). Threshold driven contagion on weighted networks. Sci. Rep. *8*, 1–10.

Vasile, F., Reina, J.J., Potenza, D., Heggelund, J.E., Mackenzie, A., Krengel, U., and Bernardi, A. (2014). Comprehensive analysis of blood group antigen binding to classical and El Tor cholera toxin B-pentamers by NMR. Glycobiology *24*, 766–778.

Vivian, J.T., and Callis, P.R. (2001). Mechanisms of tryptophan fluorescence shifts in proteins. Biophys. J. *80*, 2093–2109. https://doi.org/10.1016/S0006-3495(01)76183-8.

Vuillon, L., and Lesieur, C. (2015). From local to global changes in proteins: a network view. Curr. Opin. Struct. Biol. *31*, 1–8. https://doi.org/10.1016/j.sbi.2015.02.015.

Wagner, A. (2012). The role of robustness in phenotypic adaptation and innovation. Proc. Biol. Sci. *279*, 1249–1258. https://doi.org/10.1098/rspb.2011.2293.

Wu, F., Zhao, S., Yu, B., Chen, Y.-M., Wang, W., Song, Z.-G., Hu, Y., Tao, Z.-W., Tian, J.-H., and Pei, Y.-Y. (2020). A new coronavirus associated with human respiratory disease in China. Nature *579*, 265–269.

Xia, Y.-L., Sun, J.-H., Ai, S.-M., Li, Y., Du, X., Sang, P., Yang, L.-Q., Fu, Y.-X., and Liu, S.-Q. (2018). Insights into the role of electrostatics in temperature adaptation: a comparative study of psychrophilic, mesophilic, and thermophilic subtilisin-like serine proteases. RSC Adv. *8*, 29698–29713.

Zrimi, J., Ng Ling, A., Giri-Rachman Arifin, E., Feverati, G., and Lesieur, C. (2010). Cholera toxin B subunits assemble into pentamers - proposition of a fly-casting mechanism. PLoS One *5*, e15347.

Please cite this article in press as: Bourgeat et al., Experimental diagnostic of sequence-variant dynamic perturbations revealed by broadband dielectric spectroscopy, Structure (2021), https://doi.org/10.1016/j.str.2021.05.005

STAR★METHODS

KEY RESOURCES TABLE

REAGENT or RESOURCE	SOURCE	IDENTIFIER
Chemicals, peptides, and recombinant proteins		
Cholera toxin B-subunit pentamer	SIGMA-ALDRICH	C9903
Heat-labile enterotoxin B subunit pentamer	SIGMA-ALDRICH	E8656
Deposited data		
Cholera toxin B subunit pentamer	https://www.rcsb.org	PDB 1EEI
Heat-labile enterotoxin B subunit pentamer	https://www.rcsb.org	PDB 1LTR
Software and algorithms		
Amino acid network (AAN)	Dorantes-Gilardi et al., 2018	https://github.com/lorpac/amino_acid_network
4D-AAN	Dorantes-Gilardi et al., 2018	https://github.com/lorpac/amino_acid_network
Electrostatic dipole network (EN)	This paper	https://github.com/lorpac/amino_acid_network/blob/master/electrostatic_network.ipynb
4D-EN	Pacini et al., 2020	https://github.com/lorpac/amino_acid_network/blob/master/electrostatic_network.ipynb

RESOURCE AVAILABILITY

Lead contact

Further information and requests for resources and reagents should be directed to and will be fulfilled by the lead contact, Claire Lesieur (claire.lesieur@ens-lyon.fr).

Material availability

This study did not produce new unique reagents.

Data and code availability

Four codes are generated during this study to produce four different networks : the amino acid network (AAN), the intermolecular amino acid network (4D-AAN), the electrostatic dipole network (EN) and the intermolecular electrostatic dipole network (4D-EN). Only the EN is an addition, previous networks and codes to produce them are published. The AAN and the 4D-AAN are produced using the code available at https://github.com/lorpac/amino_acid_network. To create the full AAN, the option "dim: 'all' " should be used in the configuration file (analysis_conFigurejson), while for the 4D-AAN the option "dim: '4D' " should be used.

The EN and the 4D-EN are produced using the code available at https://github.com/lorpac/amino_acid_network/blob/master/electrostatic_network.ipynb. To create the full EN, the option "dim: 'all' " should be used in the configuration file (electrostatic_network_conFigurejson), while for the 4D-EN the option "dim: '4D' " should be used.

EXPERIMENTAL MODEL AND SUBJECT DETAILS

There are no experimental models or subjects in this study.

The Heat-Labile Enterotoxin, B subunit (LTB_5) used in this study was brought from SIGMA-ALDRICH (E8656) and according to SIGMA-ALDRICH, LTB_5 is from Escherichia coli, recombinant expressed in Pichia pastoris. The Cholera Toxin B subunit ($CtxB_5$) used in this study was brought from SIGMA-ALDRICH and according to SIGMA-ALDRICH $CtxB_5$ is produced from Vibrio cholerae.

METHOD DETAILS

Materials

Lyophilized heat labile enterotoxin B pentamer (LTB_5) purchased from Sigma Aldrich (E8656) was diluted in phosphate buffered saline (PBS; 10 mM sodium phosphate, 150 mM sodium chloride, pH 7.4) at a final concentration of 2,7 mg/mL (stock solution). The

stock solution also contained Tris buffer, NaN_3 and sodium EDTA as LTB_5 was bought from Sigma Aldrich lyophilized from a solution containing 0.05 M Tris buffer, pH 7.5, 0.2 M NaCl, 3 mM NaN3, and 1 mM sodium EDTA. LTB_5 and $CtxB_5$ are both purchased from Sigma Aldrich lyophilized from the same solution composition and prepared similarly for the BDS experiment, their dielectric responses are therefore comparable. The stock solution was aliquoted and kept at $-20°C$, frozen and thawed twice maximum for dielectric measurements. Ten-time concentrated solution of PBS solutions were purchased from BIOSOLVE and diluted 10-times in distilled water to prepare the PBS used for the toxin solution (PBSx1). In addition, the PBS solution was filtered in 22 μm filter to limit impurity contamination. The Aluminium Oxyde (AAO) Films on Al are purchased from InRedox. The AAO membrane dimensions are 10 mm * 10 mm, and they contain nanopores of 40 nm-diameters and 10-μm lengths, with 12% porosity. The AAO membrane containing the nanopores is referred to as the nanomembrane. Before use, the nanomembranes were plasma treated for twenty minutes to remove organic impurities.

Protein sample preparation

For the dielectric measurement, a protein sample at 0,025 mg/ml was used. It was prepared by diluting 2 μl of stock solution at 2,7 mg/ml in 212 μl of deionized water (final pH 6,9). The final protein solution contains protein, deionized water, salt and buffer reagents (Phosphate buffer and Tris) and some trace of sodium EDTA and NaN_3. It is worth noting that one full dielectric experiment uses as little as ~ 5 μg of toxin.

200 μl drop of sample was deposited on the nanomembrane using the drop technique, then heated at 50°C (323 K) for 15 min to evaporate the bulk water and allow entrance of the sample in the pores. The sample was then cooled down to 30°C (303 K) for 5 minutes with a speed of 2 K/min, placed between two Al electrodes of 7 mm and 40 mm diameter, respectively, and in the cell holder for measurement.

Dielectric measurements

The dielectric measurements were performed on a broadband dielectric spectrometer Novocontrol Alpha analyzer over a frequency range from 1 Hz to 10^6 Hz and over a temperature range from -80°C (193K) to 180°C (453 K). The temperature ramps were carried-out with a rate of 2K/min and a voltage of 0.2V was applied. The dielectric loss ε'', the imaginary part of the complex dielectric permittivity, was measured as a function of temperature at different frequencies. For the temperature control, a flow of pure nitrogen gas was used in a closed cryostat, providing water-free and oxygen-free experimental conditions. The thermal treatments goes from 60°C to 180°C with the following procedure. The sample is first heated to 60°C (333K) for three hours, then cooled down to -80°C (193K) (Cooling, C) and maintained for 30 min at -80°C before being heated back to 60°C (Heating, H). A cycle is composed of the cooling (C) and the heating (H) temperature measurements. A second three-hours incubation at 60°C is performed to check the stability of the sample. The temperature is then raised to 80°C for three hours followed by a cycle, and this procedure (three hours incubation and a cycle) is repeated at 100°C, 140°C and 180° where only the cooling measurement is performed. Triplicates have been done and the result of one experiment is shown. Compared to the $CtxB_5$ experiment, reproducibility of identical signals was more difficult for LTB_5 due to the lower signal resolution, which makes relaxation peaks overlapping with the conductivity signal. The transient character of the intermediates captured by BDS makes them also dependent on the kinetic and hence sensitive to the initial state of the sample in the stock solution. To solve these difficulties great care has to be taken for handling the stock solution, which should not be frozen and thawed more than twice before use. The temperature and frequency-dependencies of the relaxation processes were reproducible but the intensity between experiments could vary.

Control experiments

The dielectric response of the empty nanomembrane was measured for 10 min at 60°C and from 60°C to -80°C to control that no dielectric dispersions are detected. Likewise, the dielectric response of nanopores filled with a 200 μl drop of deionized water was measured for 10 min at 60°C and from 60°C to $-80°C$.

The native state of the toxin is checked by Trp-fluorescence before a dielectric experiment (Lesieur et al., 2002). The sample cannot be recovered from the nanopores after the BDS experiment so it is not possible to control the disassembly or unfolded state of the toxin by Trp-fluorescence and SDS-PAGE, after the dielectric measurement.

Electrostatic dipole network

The amino acid network (AAN) of the whole LTB pentamer is built using the atomic coordinates of the LTB_5 X-ray structure (PDB 1LTR) freely accessible on the RCSB website (https://www.rcsb.org/). The amino acids are the nodes of the networks linked if they have at least one atom each located within a threshold distance of 5 Å from one another. The AAN computes all atomic distances and hence models all atomic and amino acid interactions in the pentamer structure (Dorantes-Gilardi et al., 2018). The electrostatic dipole network (EN) is obtained from the AAN by keeping only opposite charged amino acids as nodes of the network linked if they have at least one atom each within 5 Å distance of one another. The EN models the Coulomb interactions between positive and negative charges in the structure. From the AAN, the intermolecular amino acid network (4D-AAN) is obtained by computing only intermolecular atomic distances between amino acids that belongs to different chains (nodes) providing the atomic and amino acid interactions involved only at the interfaces between monomers. The intermolecular electrostatic dipole network (4D-EN) is obtained from the 4D-AAN by keeping only opposite charged amino acids as nodes of the network linked if they have at least one atom each within 5 Å distance of one another. The 4D-EN models intermolecular electrostatic interactions (Pacini et al., 2020). The EN

Please cite this article in press as: Bourgeat et al., Experimental diagnostic of sequence-variant dynamic perturbations revealed by broadband dielectric spectroscopy, Structure (2021), https://doi.org/10.1016/j.str.2021.05.005

is built as the intermolecular electrostatic dipoles but considering intramolecular electrostatic dipoles (opposite charges within one monomer) as well. Dipoles computed for only one or two interfaces of the pentamer are ignored in the network as they might be due to crystallographic bias. The networks were obtained from the X-ray structure PDB 1EEI for the CtxB pentamer.

As the experiments are done at pH 6.9, the negative charges are the C-terminals, the glutamic and aspartic acids and the positive charges are the N-terminals, the lysine and the arginine residues. The orientation of the dipoles is not taken into account in the model although it could cancel out the participation of some of the dipoles to the dielectric signal when dipoles of equal strength have opposite orientation. Nevertheless, the amino acid chemical neighborhoods are anisotropic and no amino acids have same chemical environment so it appears unlikely to have dipoles with equal dielectric contribution but at opposite directions, making the approximation locally reasonable. The residue 103, a lysine in the X-ray structure PDB 1LTR of LTB_5, was ignored in the electrostatic network of LTB_5. Nevertheless, the dipole (K81, N103) is considered to be present in the BDS measurement because the residue 103 is an asparagine in the experimental LTB_5 and because the carboxyl group of the C-terminal is in the same position in the two toxin structures. There is no X-ray structure available in the Protein DataBank (https://www.rcsb.org/) for the human LTB_5 with the experimental C-terminal.

QUANTIFICATION AND STATISTICAL ANALYSIS

There are no quantification or statistical analysis in this study.